文章编号：1001－9014(2017)04－0385－04

DOI:10.11972/j.issn.1001－9014.2017.04.001

Analysis of ultraviolet and infrared dual-color focal-plane array detector based on Pt/CdS and InSb junctions

LI Qing[1,2], BAI Jie[1], LV Yan-Qiu[3], HU Wei-Da[1*], CHEN Xiao-Shuang[1], LU Wei[1]

(1. Shanghai Institute of Technical Physics, Chinese Academy of Sciences, Shanghai 200083, China;
2. University of Chinese Academy of Sciences, Beijing 100049, China;
3. China Airborne Missile Academy, Luoyang 471009, China)

Abstract: Based on finite difference time domain method (FDTD) and finite element method (FEM), the mechanism of Pt/CdS and InSb ultraviolet-infrared dual-color focal-plane arrays was investigated. It was found that a high ultraviolet photo response can be achieved for Pt/CdS Schottky junction under an ultrathin Pt top contact. Further simulations show that the ultrathin top contact can efficiently couple the infrared radiation for the dual-color focal-plane array detector. The center to center spacing of each pixel of 50 μm in the ultraviolet and infrared dual-color focal-plane array detector based on Pt/CdS and InSb junctions can significantly reduce crosstalk. Our work provides fundamental guidance for optimization and design of ultraviolet and infrared dual-color detector.

Key words: dual-color focal-plane arrays, Pt/CdS ultraviolet detector, InSb infrared detector
PACS: 42.79.Pw, 32.30.Bv, 32.30.Jc

基于 Pt/CdS 与 InSb 光伏型紫外—红外焦平面探测器的双色探测机理

李 庆[1,2], 白 杰[1], 吕衍秋[3], 胡伟达[1*], 陈效双[1], 陆 卫[1]

(1. 中国科学院上海技术物理研究所,上海 200083;
2. 中国科学院大学,北京 100049;
3. 中国空空导弹研究院, 河南 洛阳 471009)

摘要:基于新型的时域有限差分光子学分析方法联合有限元电学分析方法研究了 Pt/CdS 紫外与 InSb 红外双色焦平面阵列探测器的双色探测机理.研究发现超薄 Pt 金属膜与 CdS 形成肖特基结可以获得较大的紫外光响应并能更好耦合红外光.采用像元间距为 50 μm 的 Pt/CdS 与 InSb 键合结构,可以很好地抑制像元间的串音.结果证明了紫外-红外双色探测的可行性,该方法将为紫外—红外双色探测器的设计提供基础指导.

关 键 词:紫外—红外双色焦平面阵列;Pt/CdS 紫外探测器;InSb 红外探测器

中图分类号:O472+.8　　**文献标识码**:A

Introduction

Multicolor detection is the cutting-edge technique for third-generation infrared remote sensing. The multicolor detector can accurately distinguish between temperature and characteristics of object detection area through accessing different band signals. Dual-color focal-plane array detector can handle two wavelengths of radiation signals to remove background clutter and sunlight interference information and leave the useful information of target object which greatly improve the accuracy than monochromatic focal-plane array detector[1-3]. Since the high effective signal-to-noise ratio, dual-color focal-plane array detector shows extensive use in remote sensing, astronomy and military fields. At present dual-color detection system always relies on two kinds of focal-plane arrays or filter wheel with one focal-plane array detector to deal with two different wavelength signals. However, the system needs complicated optical elements

Received date: 2016-12-22, **revised date**: 2017-04-07　　**收稿日期**:2016-12-22, **修回日期**:2017-04-07
Foundation items:Supported by National Natural Science Foundation of China (11427807, 61521005, 11334008)
Biography:LI Qing (1991-), male, Shanghai China, master. Research area involves infrared photodetector and device simulation.
E-mail: liqing1@shanghaitech.edu.cn
* **Corresponding author**:E-mail: wdhu@mail.sitp.ac.cn

which gives rise to high cost and has difficulty in synchronizing the dual-color signal. Many groups have reported dual-color photodetectors made of mercury cadmium telluride (MCT) or quantum well double-color detector[4-10]. These dual-color devices always work in the infrared band and ignore the information in the ultraviolet band. Ultraviolet radiation window (300 ~ 400 nm) contains important information especially in the military detection field as well as the infrared window[11-12], so it is very urgent to investigate the dual-color color detectors with both ultraviolet and infrared wavelength detections. The working wavelength band of CdS is 300 nm to 500 nm, while CdS also has good transmissivity in infrared band, therefore material CdS with Pt/CdS Schottky junction is one of the best choices for ultraviolet and infrared dual-color detectors[13-14].

In this paper, the ultraviolet detector was fabricated by Pt and CdS which formed a Schottky junction in consideration of the large work function of Pt[15-16]. Due to the high quantum efficiency in the middle infrared wavelength and the mature focal plane technology, InSb was chosen as the infrared part of the dual-color focal-plane array detector. Coupling the Pt/CdS Schottky junction and InSb p-n junction, the ultraviolet and infrared dual-color focal-plane array detector was designed with relatively high dual-color detection efficiency and small crosstalk.

1 Device description and simulation

The dual-color focal-plane array detector adopted Pt/CdS schottky junction and InSb p-n junction as the ultraviolet and infrared detectors, respectively. Since the infrared radiation transmission rate of CdS is relatively high, the device was designed in the way that ultraviolet detection part in the front row was under normal incidences, and the infrared focal plane array was under back-illumination as shown in Fig. 1.

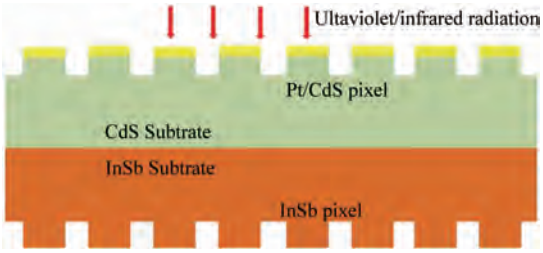

Fig. 1 The schematic of the ultraviolet/infrared dual-color focal-plane array detector
图 1 紫外—红外双色焦平面探测器示意图

Pt and CdS form a Schottky junction, however, the ultraviolet transmittance and detection efficiency are strongly affected by the thickness of Pt film. In order to obtain high detection efficiency and better ultraviolet transmittance, the spectral response of Pt/CdS ultraviolet photodetector was simulated by FDTD and FEM solution methods. Figure 2 shows the simulated structure of the ultraviolet photodetector, where the thickness of CdS is 10 μm and the CdS layer has n type doping concentration of 1.6×10^{16} cm^{-3}.

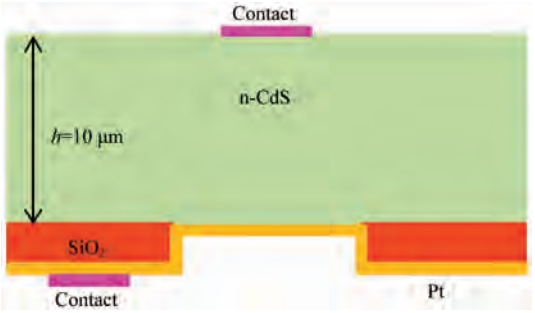

Fig. 2 The structure of Pt/CdS ultraviolet photodetector
图 2 Pt/CdS 紫外光探测器结构

Before using the simulation methods, some indispensable physical parameters of material should be calculated primarily[17]. The conductivity of metal Pt was calculated by modified Fuch-Sondheimer (F-S) theory[18]:

$$\sigma = \sigma_\infty \left(1 - \left(\frac{1}{2} + \frac{3}{4}\frac{1}{d}\right)\left[1 - k\exp\left(-\frac{\zeta}{l}d\right)\right]\exp\left(-\frac{d}{l}\right)\right), \quad (1)$$

where σ_∞ is the conductivity of the metal thickness for infinity, k is the surface scattering coefficient, d is the thickness of the film, l is the mean free path of electron and ζ the amount of grain boundary scattering. For material Pt[19-20], $\zeta = 1.15$, $l = 9.3$ nm, $\sigma_\infty = 7.58 \times 10^6$ S/m, and $k = 0.928$. The conductivity of CdS was calculated by the absorption coefficient model and the refractive index model:

$$\sigma = \frac{\alpha n}{Z_0}, \quad (2)$$

where α is the absorption coefficient, n is the refractive index and $Z_0 = \mu_0/\varepsilon_0 = 376.73\ \Omega$). Some other key parameters in simulation are shown in Table 1.

Table 1 The key parameters of Pt/CdS ultraviolet detector in simulation
表 1 模拟中 Pt/CdS 紫外探测器的关键参数

Parameters	Units	Explanations
$\omega_k = 1.244 \times 10^{15}$	s^{-1}	Pt plasma frequency
$v_k = 1.673 \times 10^{13}$	s^{-1}	Pt damping coefficient
$\varepsilon_{CdS} = 8.9$	1	CdS dielectric constant
$E_g = 2.42$	eV	CdS bandgap
$N_d = 1.6 \times 10^{16}$	cm^{-3}	N area doping
$P = 10^{-4}$	W/cm^2	Incident light energy density

Figure 3 shows relative photo response of the ultraviolet detector as a function of the thickness of CdS film, which gives information that the relative photo response grows fast when the CdS film thickness changes form 0.1 μm to 0.5 μm, while the rate become near 1 and has no longer changes when it is larger than 1 μm. So the thickness of CdS film in the simulation was chosen 10 μm far larger than 1 μm corresponding to high response. Figure 4 shows the spectral response of the ultraviolet detector with different thickness of Pt. It demonstrates that the working band of the ultraviolet detector is about 300 nm to 550 nm, and the peak of spectral response is near 500 nm. The spectral response increases rapidly with the de-

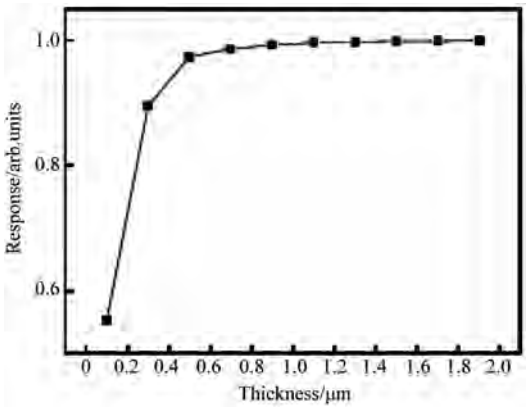

Fig. 3　Normalized photoresponse of ultraviolet detector with different thickness of CdS film
图 3　不同 CdS 厚度紫外探测器的归一化光谱响应

crease of thickness of Pt as the ultraviolet radiation can easily get in the absorption layer. When the thickness of Pt is 5 nm, the detector has the largest response, and the peak response is about 0.119 A/W which is in good agreement with the experimentally reported 0.12 A/W[15].

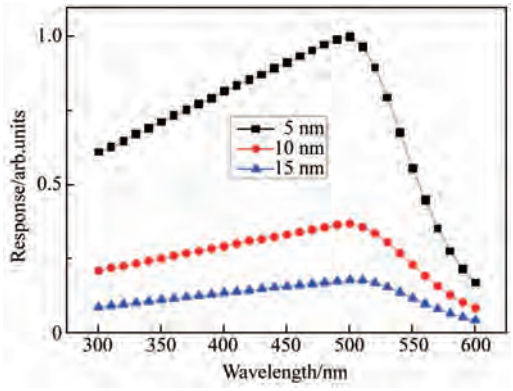

Fig. 4　Normalized photoresponse of ultraviolet detector with different thickness of Pt films
图 4　不同 Pt 金属膜厚度紫外探测器归一化光响应

According to the simulation results, the dual-color focal-plane array detector with the Pt/CdS Schottky junction as the ultraviolet detection part and InSb junction as the infrared part was designed. Figure 5 shows the schematic diagram. The thickness of CdS was designed as 4.5 μm for high spectral response and high infrared transmissivity; the n type CdS was selected and has a doping concentration of 1.6×10^{16} cm^{-3} which is easier to be implemented by epitaxial technique; the thickness of Pt film is 8 nm overall in consideration of photoresponse and transmittance; the ultraviolet photosensitive area size is 25 μm to reduce the dark current. Since infrared absorption coefficient of InSb materials is far less than the ultraviolet absorption coefficient of the CdS, and in consideration of the photo-induced carrier generation-recombination of material InSb[21-24], the thickness of InSb was designed as 9.2 μm; the n area doping concentration is 1×10^{15} cm^{-3} and the p area doping concentration is 1×10^{17} cm^{-3}; the infrared photosensitive area size is 15 μm. The array periodicity is 50 μm to reduce the crosstalk between each pixel. In the middle of the ultraviolet and infrared detector there is a SiO_2 film to prevent the electricity crosstalk between ultraviolet and infrared detectors.

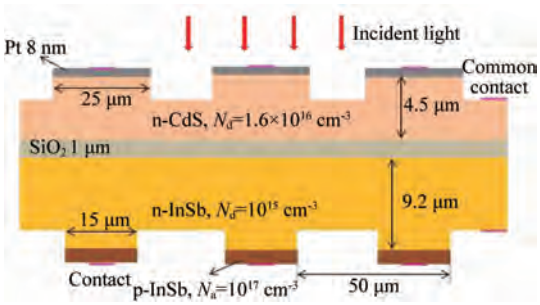

Fig. 5　Schematic diagram of ultraviolet and infrared dual-color focal-plane array detector based on Pt/CdS and InSb junctions
图 5　基于 Pt/CdS 与 InSb 光伏型紫外-红外焦平面探测器的器件结构

2　Results and discussion

In simulation, the device operating temperature was set at 77 K for smaller leakage current; the incident light density is 0.000 1 W/cm^2. Figure 6 shows the electric field distribution when the middle pixel of device is under the incident wavelength of 5 μm. It demonstrates that the infrared radiation can easily transmit the Pt/CdS detector with small attenuation which also indicates that the crosstalk between ultraviolet and infrared detectors is negligible.

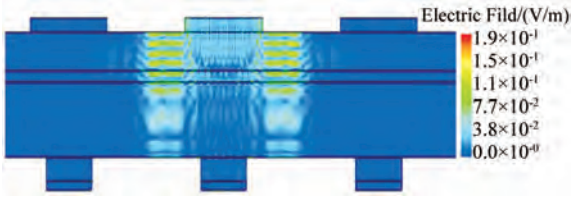

Fig. 6　The electric field distribution of ultraviolet and infrared dual-color focal-plane array detector based on Pt/CdS and InSb junctions
图 6　基于 Pt/CdS 与 InSb 光伏型紫外—红外焦平面探测器的电场分布

Figure 7(a) shows the normalized spectral response of ultraviolet and infrared dual-color focal-plane array detector based on Pt/CdS and InSb junctions. The working wavelength range of ultraviolet part is from 300 nm to 550 nm, and the peak response is 0.0403 A/W. The diffusion length of the photon-generated carrier in CdS is far less than 50 μm which is the period of the focal plane arrays, so the crosstalk of ultraviolet detector can be neglected. The working wavelength range of infrared part is from 2.9 μm to 5.7 μm, and the peak response is 1.07 A/W. Note that the spectral response shakes up near 4 μm, this may be induced by the FDTD mesh generation, time step and the incident light diffraction. Figure

7(b) shows the optics crosstalk of the infrared photodetector as a function of incident wavelength. The crosstalk of adjacent pixels is less than 17%, indicating the good independence between each pixel under different incident illuminations. The simulated results with the reasonable dual color response and crosstalk provide the feasibility of the design of the Pt/CdS ultraviolet and InSb infrared dual-color focal plane arrays.

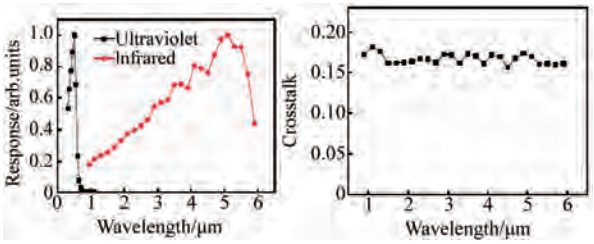

Fig. 7 (a) The spectral response of ultraviolet and infrared dual-color focal-plane arrays detector, (b) the crosstalk of InSb infrared photodetector
图7 (a)紫外—红外双色焦平面探测器的归一化光谱响应,(b) InSb红外探测器部分的串扰

3 Conclusions

In this paper, the feasibility of Pt/CdS ultraviolet and InSb infrared dual-color detection was numerically investigated by FDTD and FEM solution method. The high ultraviolet photo-response is obtained by ultrathin Pt top contact. The center to center spacing of each pixel of 50μm in the ultraviolet and infrared dual-color focal-plane array detector based on Pt/CdS and InSb junctions can significantly reduce crosstalk. The dual spectral response shows the capability of ultraviolet and infrared dual-color detection for the proposed dual-color focal-plane array detector based on Pt/CdS and InSb junctions. The method provides fundamental guidance for optimization and design of ultraviolet and infrared dual-color detector.

Acknowledgement

This work was partially supported by Natural Science Foundation of China (Grant Nos. 11427807, 61521005, 11334008)

References

[1] Chang S C, Bharathan J, Yang Y, *et al*. Dual-color polymer light-emitting pixels processed by hybrid inkjet printing [J]. *Appl. Phys. Lett*. 1998, **73**(18):2561-2563.
[2] Guo L H, Xu S H, Ma X M, *et al*. Dual-color plasmonic enzymelinked immunosorbent assay based on enzyme-mediated etching of Au nanoparticles [J], *Scientific Reports*, 2016, **6**:32755.
[3] Wang P, Liu S S, Luo W J, *et al*. Arrayed van der Waals Broadband detectors for Dual band detection[J]. *Advanced Materials*, 2017, **29**(16):1604439.
[4] Hu W D, Ye Z H, Liao L, *et al*. A 128×128 long-wavelength/mid-wavelength two-color HgCdTe infrared focal plane array detector with ultra-low spectral crosstalk [J]. *Optics Letters*, 2014,**39**(17):5130-5133.
[5] Rajavel R D, Jamba D M, Jensen J E, *et al*. Molecular beam epitaxial growth and performance of HgCdTe-based simultaneous-mode two-color detectors [J]. *Journal of Electronic Materials*, 1998, **27**(6): 747-751.
[6] Reine M B, Hairston A, O'Dette P, *et al*. Simultaneous MW/LW dual-band MOCVD HgCdTe 64×64 FPAs[J]. *Proceedings of SPIE*, 1998, **3379**: 200-212.
[7] Rajavel R D, Jamba D M, Jensen J E, *et al*. Molecular beam epitaxial growth and performance of integrated multispectral HgCdTe photodiodes for the detection of mid-wave infrared radiation [J]. *Journal of Crystal Growth*, 1998,**184**:1272-1278.
[8] Tennant W E, Thomas M, Kozlowski L J, *et al*. A novel simultaneous unipolar multispectral integrated technology approach for HgCdTe IR detectors and focal plane arrays [J]. *Journal of Electronic Materials*, 2001, **30**(6):590-594.
[9] Schneider H, Maier T, Fleissner J, *et al*. Infrared focal plane array based on MWIR/LWIR dual-band QWIPs: detector optimization and array properties [J]. *Proceedings of SPIE*, 2005, **5726**: 35-42.
[10] Gunapala S D, Bandara S V, Liu J K, *et al*. Demonstration of Megapixel Dual-Band QWIP Focal Plane Array [J]. *IEEE Journal of Quantum Electronics*, 2010, **46**(2):285-293.
[11] Li X, Zhu C X, Zhu X, *et al*. Background limited ultraviolet photodetectors of solar-blind ultraviolet detection [J]. *Applied Physics Letters*, 2013, **103**(17):896-630.
[12] Williams D L, Davey S T, Kashyap R, *et al*. Ultraviolet absorption studies on photosensitive germanosilicate preforms and fibers [J]. *Appl. Phys. Lett*. 1991, **59**(7):762-764.
[13] Liu X, Jiang L, Zou X, *et al*. Scalable integration of indium zinc oxide/photosensitive-nanowire composite thin-film transistors for transparent multicolor photodetectors array [J]. *Advanced Materials*, 2014, **26**(18):2919-2924.
[14] Miao J S, Hu W D, Guo N, *et al*. High-responsivity Graphene/InAs nanowire Heterojunction near-Infrared photodetectors with distinct photocurrent On/Off ratios [J]. *Small*, 2015, **11**(8):936-942.
[15] Qin Q, Zhu X C, Yang W Y. The development of Pt/CdS schottky barrier ultraviolet detector [J]. *Infrared Technology*, 2006, **28**(4): 234-237.
[16] Forsyth N M, Dharmadasa I M, Sobiesierski Z, *et al*. Schottky barrier to CdS and their important in Schottky barrier theories [J]. *Semiconductor Science and Technology*,1989, **4**(1):57.
[17] HU Wei-Da, LIANG Jian, YUE Fang-Yu *et al*. Recent progress of subwavelength photon trapping HgCdTe infrared detector[J]. *J. Infrared Millim. Waves*(胡伟达,梁健,越方禹,等. 新型亚波长陷光结构HgCdTe红外探测器研究进展,**红外与毫米波学报**),2016, **35**(1):25-36.
[18] Sondheimer E H. The mean free path of electrons in metals [J]. *Advances in Physics*, 1952,**1**(1):1-42.
[19] Fischer G, Hoffmann H. Oscillations of the electrical conductivity with film thickness in very thin platinum films [J]. *Solid State Commun*. 1980,**35**:793-796.
[20] Marcos de Oliveira Melo, Luciana Almeida Silva. Visible light-induced hydrogen production from glycerol aqueous solution on hybrid Pt-CdS-TiO_2 photocatalysts [J]. *Journal of Photochemistry and Photobiology A:Chemistry*, 2011, **226**: 36-41.
[21] Ashley T, Baker I M, Burke T M, et al. InSb focal plane array (FPAs) grown by molecular beam epitaxy (MBE) [J]. *Proceedings of SPIE*, 2000, **4028**:398-403.
[22] Bai J, Hu W D, Guo N, *et al*. Performance optimization of InSb infrared focal-plane arrays with diffractive microlenses [J]. *Journal of Electronic Materials*, 2014, **43**(8): 2795-2801.
[23] Guo N, Hu W D, Chen X S, *et al*. Investigation of radiation collection by the InSb infrared focal plane arrays with micro-optic structures [J]. *Journal of Electronic Materials*,2013, **42**:3181-3185.
[24] MENG Qing-Duan, LV Yan-Qiu, LU Zheng-Xiong, *et al*. Stress in InSb infrared focal plane array detector analyzed with ansys [J]. *J. Infrared Millim. Waves*(孟庆端,吕衍秋,鲁正雄, 等. InSb红外焦平面探测器结构应力的ANSYS分析,**红外与毫米波学报**), 2010, **29**(6):431-434.